Exploring critical state model outputs

Adrian Russell
School of Civil and Environmental Engineering, University of New South Wales, Sydney, Australia
David Muir Wood
Department of Civil Engineering, University of Bristol, Bristol, United Kingdom

Keywords: constitutive models, elasticity, plasticity, critical state, stiffness, instability

ABSTRACT

Constitutive models are often applied in numerical analyses involving load paths for which they have not and cannot be validated. Outputs for three critical state models are explored here. Stress response envelopes are used to contrast the incremental stiffnesses that models predict for stress and strain paths other than those used for calibration. Very different responses are observed. Plots of second order work are also presented. Negative second order work for certain strain paths indicates the potential for instability and bifurcation of response.

1 INTRODUCTION

Many constitutive models have appeared in the literature to describe the stress:strain behaviour of sands for use in numerical analyses of geotechnical engineering problems. Successful models have the potential to show bifurcated, localised response. However, models are typically validated using conventional triaxial compression tests conducted under drained and undrained conditions. These particular tests cannot cover the range of stress or strain paths experienced by soils in typical real engineering problems and numerical analysis is therefore always applying the constitutive models in regions of stress space for which they have not and cannot be validated. This paper sets out to compare the incremental response of three models to general axisymmetric combinations of incremental volumetric and shear strain. Examples of this comparison will be shown using stress response envelopes at selected stages during simulated triaxial tests. Also, through the sign of the second order work, the potential axisymmetric strain increments for which each model predicts the possibility of bifurcation of response are illustrated.

2 BASIC RELATIONSHIPS

Conventional triaxial $p':q$ notation is adopted where p' is the mean effective stress and q is the deviator stress. The corresponding strain variables are the volumetric strain ε_p and shear strain ε_q. These are related to axial and radial stresses and strains through $p' = (\sigma'_a + 2\sigma'_r)/3$, $q = \sigma'_a - \sigma'_r$, $\varepsilon_p = \varepsilon_a + 2\varepsilon_r$ and $\varepsilon_q = 2(\varepsilon_a - \varepsilon_r)/3$ where subscripts $_a$ and $_r$ denote the axial and radial components respectively. The vectorial stresses and strains are $\boldsymbol{\sigma} = [p', q]^T$ and $\boldsymbol{\varepsilon} = [\varepsilon_p, \varepsilon_q]^T$. Compression is assumed positive and rate affects are ignored. Volumetric strain is linked to specific volume v according to $\dot{\varepsilon}_p = -\dot{v}/v$. Elastic and plastic strain increments sum to give total strain increments in the normal way. Incremental elastic stresses and strains are linked through an elastic stiffness matrix $\mathbf{D}^e$ by $\dot{\boldsymbol{\sigma}} = \mathbf{D}^e \dot{\boldsymbol{\varepsilon}}^e$. The plastic stress:strain relationship is written in the general form $\dot{\boldsymbol{\varepsilon}}^p = (\mathbf{n}^T \dot{\boldsymbol{\sigma}})\mathbf{m}/h$ where $\mathbf{n} = [n_p, n_q]^T$ is the unit normal vector at the current stress state controlling the direction of loading, $\mathbf{m} = [m_p, m_q]^T$ is the unit direction of plastic flow at the current stress state and h is the hardening modulus. Using $\mathbf{D}$ to denote the elastic-plastic stiffness matrix, the elastic-plastic stress:strain relationship is:

$$\dot{\boldsymbol{\sigma}} = \left(\mathbf{D}^e - \frac{\mathbf{D}^e \mathbf{m} \mathbf{n}^T \mathbf{D}^e}{h + \mathbf{n}^T \mathbf{D}^e \mathbf{m}} \right) \dot{\boldsymbol{\varepsilon}} = \mathbf{D} \dot{\boldsymbol{\varepsilon}} \qquad (1)$$

3 STRESS RESPONSE ENVELOPES AND SECOND ORDER WORK

In numerical analysis the principal purpose of constitutive models is to provide a description of the local generalised incremental stiffness. Stress response envelopes provide a compact way of illustrating this incremental stiffness at a particular soil state [Gudehus, 1979; Muir Wood, 2004]. Consider a number of identical soil samples each having experienced exactly the same loading history. Each sample is then subjected to a different member of a set of strain increments $\dot{\boldsymbol{\varepsilon}} = \left[\dot{\varepsilon}_p, \dot{\varepsilon}_q\right]^T$ that define a unit strain vector ($\dot{\varepsilon}_p = \cos\theta$ and $\dot{\varepsilon}_q = \sin\theta$ for $0^\circ \le \theta \le 360^\circ$, with θ defined in an anticlockwise direction from the horizontal). Equation (1) is then used to obtain the corresponding incremental values of $\dot{p}'$ and $\dot{q}$ for any given model. The curve linking the values of $\dot{p}'$ and $\dot{q}$ for all different values of θ is a stress response envelope corresponding to the particular loading history (Figure 1). At selected points round the stress response envelope, scaled vectors are drawn to indicate the combinations of $\dot{\varepsilon}_p$ and $\dot{\varepsilon}_q$ that were used to establish those incremental stresses. The numerical values on the axes of the stress response envelope have no meaning other than to indicate the relative magnitudes of $\dot{p}'$ and $\dot{q}$. The further the envelope lies from the origin (the initial common stress state) the stiffer the soil response for that combination of $\dot{\varepsilon}_p$ and $\dot{\varepsilon}_q$.

It is generally accepted that for materials which do not follow the constraint of associated flow, so that **n** ≠ **m**, there is the possibility of bifurcation of response, with the development of internal heterogeneities or localisations, before the peak of the stress:strain relationship. Such a possibility is also supported by experimental evidence. Hill's (1958) second order work criterion can be used to indicate the possibility of instability developing. Second order work per unit volume ($\ddot{W}$) is:

$$\ddot{W} = \dot{\boldsymbol{\sigma}}^T \dot{\boldsymbol{\varepsilon}} = \dot{p}'\dot{\varepsilon}_p + \dot{q}\dot{\varepsilon}_q \qquad (2)$$

and, according to Hill (1958), a stable condition exists when $\ddot{W} > 0$. For the sample in Figure 1 we can calculate the value of $\ddot{W}$ for each strain probe and generate a radial plot of scaled values of $\ddot{W}$ (Figure 2) such that negative values plot inside and positive values plot outside a unit reference circle (of radius 1) [Laouafa & Darve, 2002]. The scale used for plotting values of $\ddot{W}$ is arbitrary – it is the sign of $\ddot{W}$ which indicates the possibility of instability.

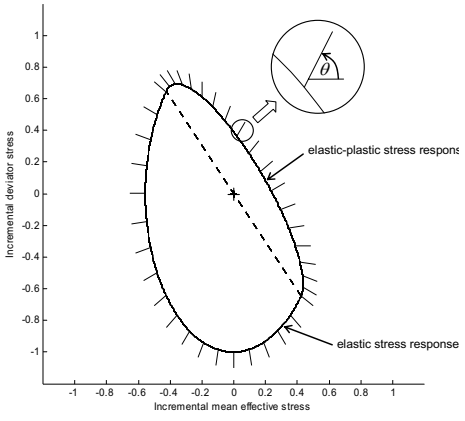

Figure 1: A stress response envelope with strain increment vectors at θ = 10° intervals

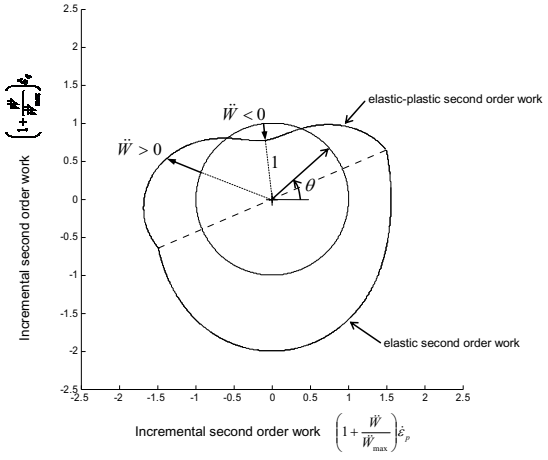

Figure 2: A second order work diagram with a unit reference circle corresponding to $\ddot{W} = 0$

4 THE CONSTITUTIVE MODELS

The three constitutive models considered here differ primarily in the assumed form of their hardening rules and the shape of their loading or yield surfaces. However, the models possess many

underlying similarities and some subtle changes have been made in order to bring the models into some conformity and identify key points of difference. The differences are briefly described below. Reference should be made to Gajo & Muir Wood (1999), Russell & Khalili (2006) and Boukpeti & Drescher (2000) for details of each model in its original creation.

4.1 Elasticity, loading and yield surfaces

In all three models isotropic elasticity is assumed, defined by the tangent bulk and shear moduli. It has been assumed that isotropic elastic unloading and reloading are defined by linear relationships of slope κ in the v ~ lnp′ plane so that bulk modulus K is broadly proportional to p′.

A yield surface bounds a region of stress space within which the response is purely elastic. A loading surface distinguishes between loading and unloading, with different incremental stiffnesses. However, the response at the commencement of unloading is purely elastic. The current stress state always lies on the loading/yield surface. For Severn-Trent, the yield surface has a frictional character, defining an elastic 'wedge' in the q ~ p′ plane (Figure 3). In the Unified model and Superior sand the loading surfaces have tear drop shapes and a parametric size p'_c (Figure 3).

4.2 Flow rule

The flow rule defines the ratio d of incremental plastic volumetric strain and plastic shear strain as a function of stress ratio $\eta = q/p'$. The same form is used for all three models

$$d = \dot{\varepsilon}_p^p \big/ \dot{\varepsilon}_q^p = (1 + k_d \xi) M_{cs} - \eta \qquad (3)$$

where M_{cs} is a function of critical state strength, k_d is a material parameter and ξ is the state parameter of Been & Jefferies (1985) – the difference between the current and critical state values of void ratio at the current mean stress (Figure 4).

4.3 Hardening rules

All three models adopt elements of bounding surface plasticity in their hardening rules in order to define a steady fall of stiffness from the current stress state towards some asymptotic ultimate state. For Severn-Trent sand distortional hardening is assumed to occur according to a simple hyperbolic relationship linking η and plastic shear strain ε_q^p. This relationship describes the steady mobilisation of strength towards the current peak strength η_p which itself varies as a function of ξ. Within the Unified model and Superior sand the bounding surface has the same shape as the loading surface. h is defined as two additive parts, one part being a direct function of ε_p^p (as well as ε_q^p for Superior sand) with the other being an arbitrary decreasing function of the distance between the two surfaces. In all three models $m_p = 0$, h = 0 and $\det \mathbf{D} = 0$ at the critical state, so that reaching the critical state is controlled by interaction of the flow rule and hardening rule.

4.4 The critical state

The critical state acts as an asymptotic condition towards which the state of the soil approaches with increasing plastic shear strain. As implemented here, the CSL is defined as locally straight in the v ~ lnp′ compression plane for Severn-Trent and Superior sand:

$$v = \Gamma_0 - \lambda_0 \ln p' \qquad (4)$$

where λ_0 and Γ_0 are the slope of the CSL and the specific volume at p′ = 1kPa. In order to demonstrate the influence that the shape of the CSL can have on the simulated response, a more elaborate CSL is implemented in the Unified model, with three linear segments in the v ~ lnp′ compression plane, defined by the six material parameters λ_0, Γ_0, v_{cr}, λ_{cr}, v_f and λ_f shown in Figure 4. For all three models the CSL in the q ~ p′ plane is assumed to be a straight line through the origin of slope M_{cs}. M_{cs} is a function of the critical state friction angle in triaxial compression.

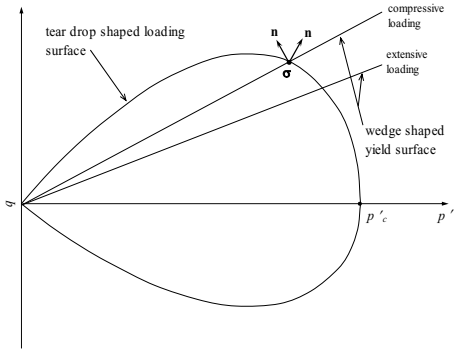

Figure 3: Different shapes for loading surfaces in the q ~ p′ plane, along with loading vectors at the current stress state

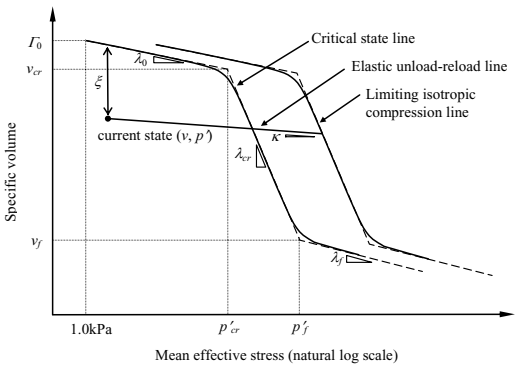

Figure 4: A general critical state line for sands in the v ~ lnp′ plane and an elastic unload-reload line

5 COMPARISONS

Figure 5 presents experimental results of Benahmed (2001) and model simulations for two conventional triaxial compression tests on Hostun sand: a drained test on a loose sample and an undrained test on a medium dense sample. Selected stress response envelopes and second order work diagrams are shown in Figure 6. The dotted line through the origin on the stress response envelopes & second order work diagrams shows the orientation of the loading-unloading boundary.

For drained triaxial test 12, with the initial conditions $p'_0 = 400$ kPa and $v_0 = 1.899$, it can be seen that all models simulate the results reasonably well. The only significant difference is that the Unified model slightly over predicts the volumetric compression. Undrained triaxial test 54, with initial conditions $p'_0 = 200$ kPa and $v_0 = 1.744$, shows considerable suppressed dilation leading to a tendency for p′ to increase. The Unified model simulates this aspect of the results reasonably well and the other two models are less successful, primarily as a result of the different CSLs that the models use. As implemented here, Severn-Trent sand and Superior sand use a single linear CSL in the v ~ lnp′ plane. In undrained simulations the stress states strive to reach the CSL at an unrealistically large value of p′ corresponding to the initial specific volume $v_0 = 1.744$. Using the three section CSL shown in Figure 4 in the Unified model allows the stress state to move towards a much lower and more realistic value of p′.

Concentrating on simulation of conventional triaxial tests shows differences in detail between the models but produces representations of the experimental observations which are broadly of similar quality: major differences arise from the very different formulation of the CSL in the Unified model. However, comparison of stress response envelopes (Figure 6) shows very clearly that, even if the incremental stiffness for continuation through a given test is similar, for any other incremental path which produces plastic deformation the incremental stiffness will be very different. For example, Figure 6 shows response envelopes at strain $\varepsilon_q = 0.005$ in drained test 12. The response for continuation of the drained stress path, with $\dot{q}/\dot{p}' = 3$, is essentially identical for all three models: the three response envelopes (approximately) intersect for this stress increment direction and have similar strain vectors. However, for other directions of stress path the response is predicted to be quite different. The orientation of the elastic-plastic (low stiffness) part of the response envelope is primarily related to the local slope of the loading-unloading boundary for each model. Severn-Trent sand, an extended Mohr-Coulomb model, has a boundary that is much steeper and orientated in a direction opposite to the boundaries of the other models. For a purely hydrostatic stress increment ($\dot{q}/\dot{p}' = 0$) in compression Severn-Trent sand and the Unified model predict stiff, purely elastic response whereas Superior sand predicts less stiff elastic-plastic response: the stress response envelope is closer to the initial stress state for this particular stress increment direction. The situation is reversed for an unloading hydrostatic stress increment. For an undrained increment ($\dot{\varepsilon}_p/\dot{\varepsilon}_q = 0$) all three models predict elastic-plastic response in the drained test but the predicted

stress increment ratios are quite different: $\dot{q}/\dot{p}' = 0.6$, -0.1 and -1.1 for Severn-Trent sand, Unified model and Superior sand respectively. However, by the time the strain has reached ε_q = 0.05 the differences between the models are rather small – the sand has reached a low stiffness close to the critical state. Broadly similar conclusions can be drawn for the incremental response during undrained test 54. There are greatly contrasting incremental responses at a strain of 0.001 but rather similar responses at 0.005.

Consideration of the second order work diagrams (Figure 6) shows that the tendencies to instability predicted by the models are also very different. For undrained test 54, the progressive development of potential instability through the test, as revealed by the second order work diagrams, is rather similar in the three models. However, for drained test 12 Severn-Trent sand shows negative second order work at about ε_q = 0.003, then the Unified model at about ε_q = 0.005 and then Superior sand at about ε_q = 0.011. While second order work is positive in the direction of continuing loading, for steeper strain paths, and paths with modest imposed volumetric expansion (for strain increment directions in the range $\theta = 85^\circ$ to 145°), second order work is negative for Severn-Trent sand at a strain of 0.005. These directions include $\theta = 90^\circ$ indicating the potential for undrained instability or static liquefaction which could be triggered by some minor strain perturbations.

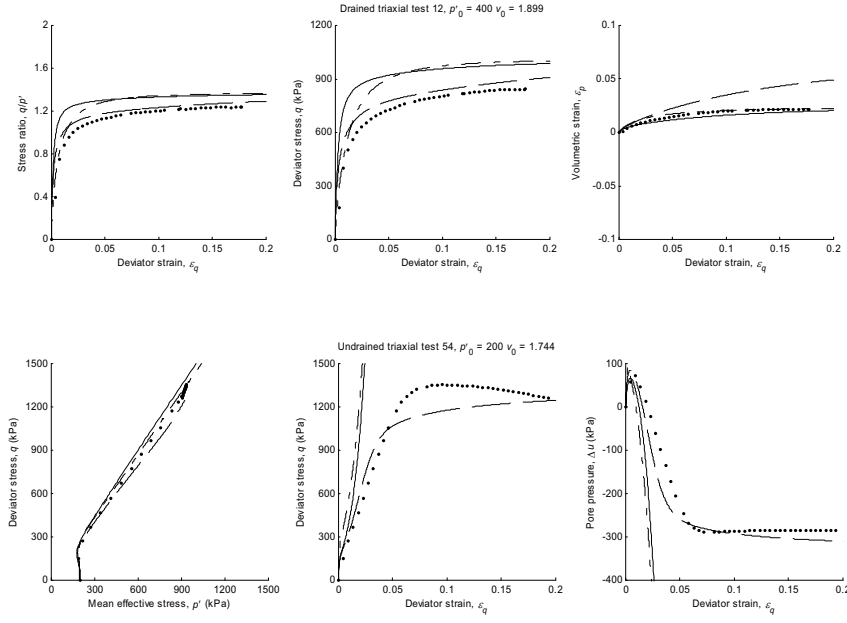

Figure 5: Experimental results and model simulations for triaxial tests 12 and 54. The solid symbols represent the experimental data, the continuous line, dashed line and dash-dot line represent the Severn-Trent sand, Unified model and Superior sand simulations respectively

6 CONCLUSIONS

Three models have been compared here. They are all elastic-plastic models and therefore have common ingredients governing their mathematical structure. Their principal differences lie in the loading or yield functions, and the hardening rule. The shape of the locus of ultimate critical states in the compression plane can have a dramatic effect on the predictions of pore pressure development in undrained tests. Major differences between the stress response envelopes and expectations of bifurcation of response can be linked with the local tangent to the loading or yield surface at the current stress state. Models calibrated with data from limited stress paths may produce unexpected predictions on uncalibrated paths.

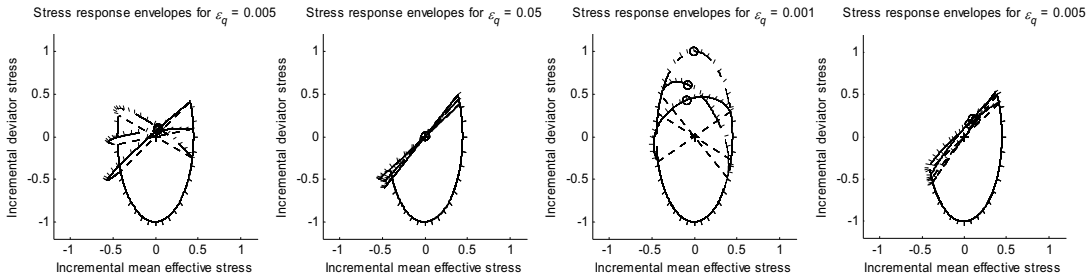

(a) Drained triaxial test 12

(b) Undrained triaxial test 54

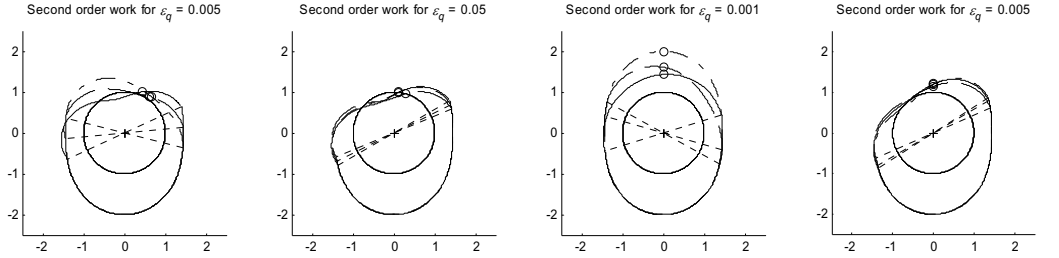

Figure 6: Stress response envelopes and second order work plots for (a) drained triaxial test 12 at ε_q = 0.005 and 0.05, and (b) undrained triaxial test 54 at ε_q = 0.001 and 0.005

REFERENCES

Been, K. & Jefferies, M. G. (1985). A state parameter for sands. *Géotechnique* **35**(2), 99-112.

Benahmed, N. (2001). *Comportement mécanique d'un sable sous cisaillement monotone et cyclique*. Thèse de Doctorat, Ecole Nationale des Ponts et Chaussées, France.

Boukpeti, N. & Drescher, A. (2000). Triaxial behaviour of refined Superior sand model. *Computers and Geotechnics* **26**, 65-81.

Gajo, A. & Muir Wood, D. (1999). Severn-Trent sand: a kinematic-hardening constitutive model: the *q–p* formulation. *Géotechnique* **49**(5), 595–614.

Gudehus, G. (1979). A comparison of some constitutive laws for soils under radially symmetric loading and unloading. *Proc. 3rd Int. Conf. Num. Meth. Geomech.,* A.A.Balkema, 1309-1323.

Hill, R. (1958). A general theory of uniqueness and stability in elastic-plastic solids. *J. Mech. Phys. Solids* **6**, 236-249.

Laouafa, F. & Darve, F. (2002). Modelling of slope failure by a material instability mechanism. *Comput. and Geotechnics* **29**, 301-325.

Muir Wood, D. (2004). *Geotechnical modelling*. E. & F. N. Spon. ISBN: 0419237305.

Russell, A. R. & Khalili, N. (2006). A Unified bounding surface plasticity model for unsaturated soils. *Int. J. Numer. Anal. Meth. Geomech.* **30**, 181-212.